Available online at www.sciencedirect.com

ScienceDirect

IFAC Papers Online CONFERENCE PAPER ARCHIVE

IFAC PapersOnLine 56-2 (2023) 899–904

Guided control of a human driver via an automated vehicle

Bence Szaksz *, **Gábor Orosz** **, and **Gábor Stépán** ***

* *Department of Applied Mechanics, MTA-BME Lendület "Momentum" Global Dynamics Research Group, Faculty of Mechanical Engineering, Budapest University of Technology and Economics, Budapest, H 1111, Hungary (e-mail: szaksz@mm.bme.hu).*
** *Department of Mechanical Engineering, and Department of Civil and Environmental Engineering, University of Michigan, Ann Arbor, MI 48109, USA (e-mail: orosz@umich.edu)*
*** *Department of Applied Mechanics, Faculty of Mechanical Engineering, Budapest University of Technology and Economics, Budapest, H 1111, Hungary, (e-mail: stepan@mm.bme.hu)*

Abstract: The present work investigates the dynamics of a guided control situation when an automated vehicle is traveling in front of a human-driven vehicle, while the control of the automated vehicle contains the combination of a cruise control term and a backward looking term. The plant and string stability conditions of the underlying dynamical system are determined. The relevant time delays are taken into account and stability charts are presented for various delay combinations. A simple approximation of the string stable domain is proposed.

Keywords: Autonomous vehicles; human and vehicle interaction; multi-vehicle systems; time-delay systems; stability of delay systems

1. INTRODUCTION

With the increasing number of vehicles on roads, traffic congestions are formed more and more often, and the number of potential safety critical situations also increases. Autonomous driving systems may help in both cases (Caveney (2010); Chan et al. (2012)); there are several studies about platoons of connected vehicles, which provide fast and safe transport (Lidström et al. (2012); Milanés et al. (2013); Ploeg et al. (2013a); Öncü et al. (2014)). Although, the human-driven vehicles remain present in the near future, some of these may be connected to a few automated vehicles, which can benefit the automated vehicles and also provide certain levels of traffic control. In case of connected cruise control (CCC), the automated vehicle is connected to some human-driven vehicles ahead (Qin et al. (2016); Orosz (2016)). In case of adaptive traffic control (ATC), the automated vehicle is connected to some human-driven vehicles behind (Molnár et al. (2023)). Finally, in case of connected traffic control (CTC) or leading cruise control (LCC), the automated vehicle is connected to vehicles both behind and ahead (Molnár et al. (2023); Wang et al. (2021)).

The traffic dynamics can be described in a vehicle-based, also called Lagrangian coordinate system (Čičić and Johansson (2018); Yu et al. (2018); Laval and Leclercq (2013); Molnár et al. (2021)), which is nowadays more popular than the location-based Eulerian approaches (Bekiaris-Liberis and Delis (2020); Yu et al. (2018)). The corresponding dynamics presents intricate phenomena due to the relevant time delays in the control; this was first introduced by Bando et al. (1998) and it is still a relevant research topic (Orosz and Stépán (2006); Wang et al. (2018); Loizou et al. (2021)).

The present paper investigates the simplest traffic control, when an automated vehicle (AV) runs in front of a human-driven vehicle (HV). The AV aims to travel according to a reference velocity but it senses also the velocity of the HV and so provides a guided control for the human driver. After introducing the model, the stability of the system is analyzed for various control parameters. Then the effects of the relevant time delays are taken into account in the control of both the HV and the AV. Finally, simple suggestions are provided to guide the tuning process of the control gains of the AV.

2. MODELING

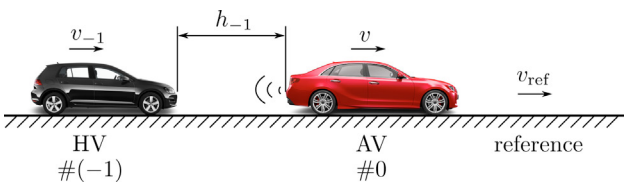

Fig. 1. Single-lane guided car following.

The investigated guided car following model is visualized in Fig. 1: an AV of velocity v aims to cruise according to a possibly time-dependent reference velocity v_{ref} while a HV follows it with velocity v_{-1}; the headway between the two vehicles is denoted by h_{-1}. The dynamics of the simplified model assumes the form:

10.1016/j.ifacol.2023.10.1679

$$\dot{h}_{-1} = v - v_{-1}\,, \tag{1}$$
$$\dot{v}_{-1} = \alpha(V(h_{-1}) - v_{-1}) + \beta(W(v) - v_{-1})\,, \tag{2}$$
$$\dot{v} = \hat{\beta}(v_{\rm ref} - v) + \beta_{-1}(W(v_{-1}) - v)\,, \tag{3}$$

where

$$W(v) = \min(v, v_{\max}), \tag{4}$$

is the velocity saturation function and

$$V(h) = \min(\max(0, F(h), v_{\max})), \tag{5}$$

is the range policy. Thus, the gains $\hat{\beta}$ and β_{-1} determine the control law of the AV. The gains α and β describe the assumed control strategy of the human driver, who also takes into account the headway h_{-1} and aims to drive according to the function $F(h)$ (see Bando et al. (1998)) if the headway is within the range $h_{\rm st} < h_{-1} < h_{\rm go}$. If the distance between the two vehicles is below $h_{\rm st}$ then the driver tries to stop, while if it is larger than $h_{\rm go}$ then the vehicle ahead is far enough to travel with a predefined maximum velocity $v_{\max}$ (see Molnár et al. (2020, 2023)).

3. CONTROL DESIGN

In case of the steady state motion, both vehicles travel with velocity $v_{\rm ref}$ and the corresponding headway is determined by the inverse of the range policy: $h^\star_{-1} = V^{-1}(v_{\rm ref})$. The state vector $\mathbf{x} = [\tilde{h}_{-1}\ \tilde{v}_{-1}\ \tilde{v}]^{\rm T}$ is defined by

$$\tilde{h}_{-1} = h_{-1} - h^\star_{-1},\ \tilde{v}_{-1} = v_{-1} - v_{\rm ref},\ \tilde{v} = v - v_{\rm ref}\,, \tag{6}$$

which leads to the linearized governing equations:

$$\dot{\mathbf{x}} = \mathbf{A}\mathbf{x} + \mathbf{B}v_{\rm ref}\,, \tag{7}$$
$$y = \mathbf{C}\mathbf{x}\,. \tag{8}$$

Here, the output y is the velocity of the HV and the coefficient matrices are

$$\mathbf{A} = \begin{bmatrix} 0 & -1 & 1 \\ \alpha\kappa & -(\alpha+\beta) & \beta \\ 0 & \beta_{-1} & -(\hat{\beta}+\beta_{-1}) \end{bmatrix},\ \mathbf{B} = \begin{bmatrix} 0 \\ 0 \\ \hat{\beta} \end{bmatrix},\ \mathbf{C} = [0\ 1\ 0]\,, \tag{9}$$

where κ is the slope of the range policy function $V(h)$ at the equilibrium, and so, it is approximately the inverse of the time headway.

Since the reference velocity can be a function of time, the above system is non-autonomous and its stability can be investigated in two aspects: the system is called plant stable if it is stable for constant $v_{\rm ref}$, and it is called string stable if it is plant stable and the perturbations in $v_{\rm ref}$ do not lead to increased oscillations in the output y (Besselink and Johansson (2017); Swaroop and Hedrick (1996); Ploeg et al. (2013b)).

3.1 Plant stability

The characteristic function assumes the form:

$$D(s) := \det(s\mathbf{I} - \mathbf{A}) = s^3 + (\alpha + \beta + \hat{\beta} + \beta_{-1})s^2 + (\alpha\hat{\beta} + \alpha\beta_{-1} + \beta\hat{\beta} + \alpha\kappa)s + \alpha\kappa\hat{\beta}\,. \tag{10}$$

If all its zeros have negative real part, the system is plant stable. Substituting $s = 0$ into the characteristic equation $D(s) = 0$, and assuming $\alpha > 0$ and $\kappa > 0$, the static stability (possible saddle-node bifurcation) boundary is located at

$$\hat{\beta} = 0\,. \tag{11}$$

Substitution of $s = {\rm j}\Omega$ in (10), leads to the parametric form of the dynamic stability (possible Hopf bifurcation) boundary

$$\beta_{-1}(\Omega) = -\frac{\Omega^4 + ((\alpha+\beta)^2 - 2\alpha\kappa)\Omega^2 + \alpha^2\kappa^2}{\beta\Omega^2 + \alpha^2\kappa}\,, \tag{12}$$
$$\hat{\beta}(\Omega) = \frac{\Omega^4 + \alpha(\alpha+\beta-\kappa)\Omega^2}{\beta\Omega^2 + \alpha^2\kappa}\,, \tag{13}$$

where the parameter Ω is the angular frequency with which the system looses its stability. Substituting $\Omega = 0$, the curve starts from the point $\beta_{-1} = -\kappa$, $\hat{\beta} = 0$ and its slope tends to -1 for large values of Ω (see Fig. 2).

A typical stability chart can be seen in the upper left panel of Fig. 2. The stability boundary curves are given in (11)-(13), the stable region can be identified with the Routh-Hurwitz criterion; both the light and dark gray regions are plant stable, which implies that not only the whole positive quadrant of the β_{-1}, $\hat{\beta}$ plane is stable but the backward looking gain β_{-1} can take even negative values if $\hat{\beta}$ is large enough. The smaller panels in the first and third rows show the characteristic roots at six distinct parameter points.

3.2 String stability

To investigate the string stability, the transfer function should be determined between the reference velocity and the velocity of the HV:

$$T(s) = \mathbf{C}(s\mathbf{I} - \mathbf{A})^{-1}\mathbf{B} =: \frac{N(s)}{D(s)}\,. \tag{14}$$

Here, the denominator $D(s)$ is identical to the characteristic function (10), and the numerator assumes the form

$$N(s) = s\beta\hat{\beta} + \alpha\kappa\hat{\beta}\,. \tag{15}$$

By definition, the system is string stable if it is plant stable and

$$|T({\rm j}\omega)| < 1,\ \text{for all}\ \omega > 0\,. \tag{16}$$

Let us introduce

$$P(\omega) = \frac{1}{\omega^2}\left(|N({\rm j}\omega)|^2 - |D({\rm j}\omega)|^2\right)\,, \tag{17}$$

with which the definition (16) can be rewritten as

$$P(\omega) < 0,\ \text{for all}\ \omega > 0\,, \tag{18}$$

where

$$P(\omega) = -\omega^4 - \Big((\alpha+\beta)^2 + (\hat{\beta}+\beta_{-1})^2 - 2\alpha\kappa + 2\beta\beta_{-1}\Big)\omega^2 - \alpha\Big(2\hat{\beta}(\hat{\beta}+\beta_{-1})(\beta-\kappa) + \alpha\big((\hat{\beta}+\beta_{-1})^2 + 2\kappa\beta_{-1} + \kappa^2\big)\Big). \tag{19}$$

The critical parameter combinations at which the system may loose string stability are the cases when

$$P(0) = 0\,, \tag{20}$$

and

$$P(\omega^\star) = 0\,, \qquad \left.\frac{{\rm d}P(\omega)}{{\rm d}\omega}\right|_{\omega=\omega^\star} = 0 \quad \text{for}\ \omega^\star > 0\,. \tag{21}$$

Expressing the $\omega = 0$ string stability boundary for $\hat{\beta}$ yields

$$\hat{\beta} = -\beta_{-1}\frac{\alpha+\beta-\kappa}{\alpha+2\beta-2\kappa} \pm \frac{\sqrt{\beta_{-1}^2(\alpha+\beta-\kappa)^2 - \alpha(\alpha+2\beta-2\kappa)(\beta_{-1}+\kappa)^2}}{\alpha+2\beta-2\kappa}\,, \tag{22}$$

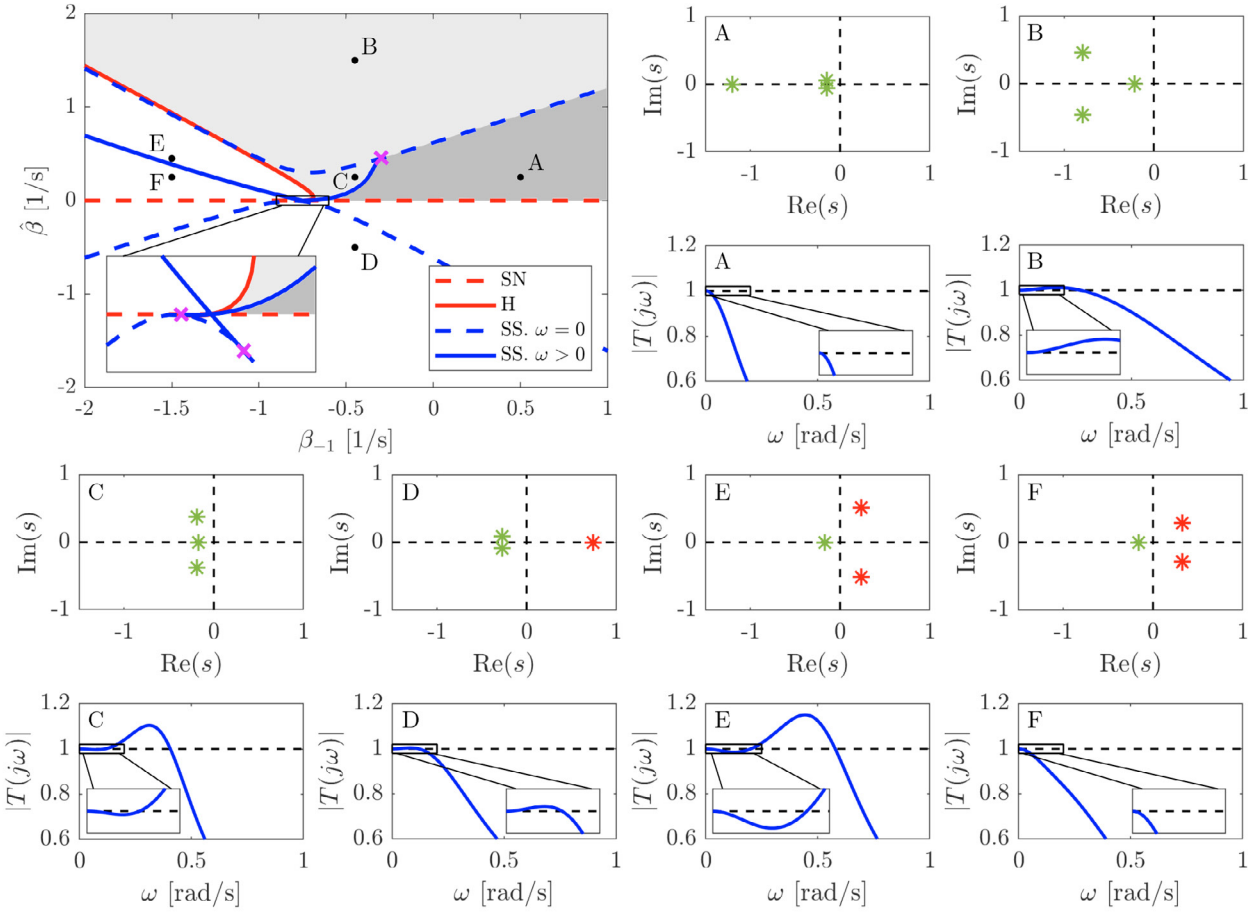

Fig. 2. The upper left panel presents a stability chart in the plane of the control gains of the AV (for HV parameters $\alpha = 0.15$ 1/s, $\kappa = 0.8$ 1/s, $\beta = 0.6$ 1/s). The light and dark gray regions are both plant stable, while only the dark gray area is string stable. The small panels present the characteristic roots and the norms of the transfer function for various control gain combinations selected from the stability chart. Point A is a plant and string stable configuration, B and C are only plant stable, while the points D, E and F are all unstable in both senses even though in case of F, the norm of the transfer function remains below 1.

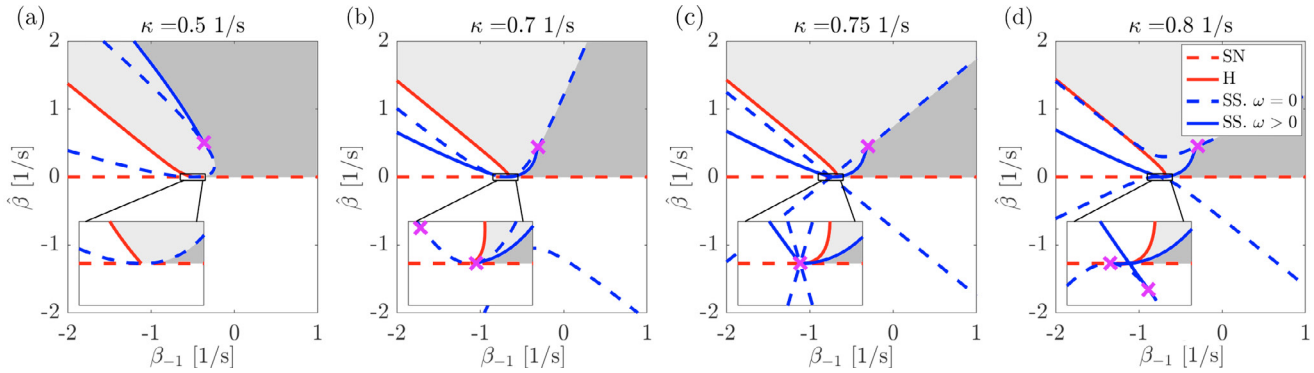

Fig. 3. Stability charts for various values of κ (the inverse of the time headway) with human gains $\alpha = 0.15$ 1/s, $\beta = 0.6$ 1/s. The light and dark gray regions are both plant stable, while only the dark gray area is string stable.

which forms two parabolas (see the blue dashed curves in Fig. 2).

In case of human drivers, $\kappa \approx \alpha+\beta$ (see Ge et al. (2018)). If they are exactly equal then (22) simplifies to the expression of two straight lines:

$$\hat{\beta} = \pm(\beta_{-1} + \alpha + \beta)\,. \tag{23}$$

The $\omega > 0$ string stability boundary can also be determined in a lengthy closed form that is not presented here; the corresponding boundary curves are plotted with blue solid lines in the stability chart of Fig. 2. As ω increases from zero, these blue curves detach from the dashed blue curves; the detachment points are marked with purple crosses. There, in addition to (20),

$$\left.\frac{\mathrm{d}^2 P(\omega)}{\mathrm{d}\omega^2}\right|_{\omega=0} = 0 \tag{24}$$

also fulfils leading to further lengthy expressions. For $\kappa = \alpha + \beta$, these simplify to

$$\beta_{-1} = -\alpha - \beta,\ \hat{\beta} = 0 \text{ and } \beta_{-1} = -\frac{\beta}{2},\ \hat{\beta} = \alpha + \frac{\beta}{2}\ , \tag{25}$$

which is presented in panel (c) of Fig. 3.

In Fig. 2, the string stable region is colored dark gray. The smaller panels in the second and fourth rows show the norm of the transfer function (14) for six different parameter combinations.

Figure 3 shows stability charts for various, practically relevant κ values. Increasing κ, that is, considering more and more aggressive human drivers, the plant stable region changes just slightly, but the string stable area shrinks significantly. Furthermore, panel (c) presents the special configuration $\kappa = \alpha + \beta$, where the $\omega = 0$ string stability curves become straight lines.

4. EFFECTS OF TIME DELAYS

In real scenarios, both the control of the HV and the control of the AV are subjected to time delay originating from the human reaction time, processing time and actuation delay. Denoting these delays by τ and σ corresponding to the HV and to the AV, respectively, the equation of motion assumes the form

$$\dot{\mathbf{x}}(t) = \mathbf{A}_0\mathbf{x}(t) + \mathbf{A}_\tau\mathbf{x}(t-\tau) + \mathbf{A}_\sigma\mathbf{x}(t-\sigma) + \mathbf{B}v_{\mathrm{ref}}\,, \tag{26}$$

where

$$\mathbf{A}_0 = \begin{bmatrix} 0 & -1 & 1 \\ 0 & 0 & 0 \\ 0 & 0 & 0 \end{bmatrix}, \quad \mathbf{A}_\tau = \begin{bmatrix} 0 & 0 & 0 \\ \alpha\kappa & -(\alpha+\beta) & \beta \\ 0 & 0 & 0 \end{bmatrix}, \quad \mathbf{A}_\sigma = \begin{bmatrix} 0 & 0 & 0 \\ 0 & 0 & 0 \\ 0 & \beta_{-1} & -(\hat{\beta}+\beta_{-1}) \end{bmatrix}. \tag{27}$$

4.1 Plant stability

The corresponding characteristic function is a quasi-polynomial:

$$\begin{aligned} D(s) &:= \det(s\mathbf{I} - \mathbf{A}_0 - \mathbf{A}_\tau \mathrm{e}^{-s\tau} - \mathbf{A}_\sigma \mathrm{e}^{-s\sigma}) \\ &= s^3 + (\alpha+\beta)s^2\mathrm{e}^{-s\tau} + (\hat{\beta}+\beta_{-1})s^2\mathrm{e}^{-s\sigma} \\ &+ (\beta\hat{\beta} + \alpha\hat{\beta} + \alpha\beta_{-1})s\mathrm{e}^{-s(\tau+\sigma)} + \alpha\kappa s\mathrm{e}^{-s\tau} \\ &+ \alpha\kappa\hat{\beta}\mathrm{e}^{-s(\tau+\sigma)}, \end{aligned} \tag{28}$$

and the stability analysis can be done with the help of the D-subdivision method (Stépán (1989)). Assuming $\alpha > 0$ and $\kappa > 0$, the saddle-node boundary is the same as before:

$$\hat{\beta} = 0\,. \tag{29}$$

Substituting $s = \mathrm{j}\Omega$ into the characteristic equation (28), the Hopf boundary curves can be given as a function of Ω:

$$\beta_{-1}(\Omega) = \cos(\Omega\sigma)\frac{a(\Omega)}{c(\Omega)}\,, \quad \hat{\beta}(\Omega) = \frac{b(\Omega)}{c(\Omega)}, \tag{30}$$

where

$$\begin{aligned} a(\Omega) &= -\Omega^4 + 2\Omega^3(\alpha+\beta)\sin(\Omega\tau) \\ &- \Omega^2\big((\alpha+\beta)^2 + 2\alpha\kappa\cos(\Omega\tau)\big) - \alpha^2\kappa^2\,, \end{aligned} \tag{31}$$

$$\begin{aligned} b(\Omega) &= \Omega^4\cos(\omega\sigma) + \Omega^2(\alpha^2+\alpha\beta)\cos(\Omega\sigma) \\ &- (\alpha+\beta)\Omega^3\sin(\Omega(\tau-\sigma)) - \alpha\Omega^3\sin(\Omega(\tau+\sigma)) \\ &- \alpha\kappa\Omega^2\cos(\Omega(\tau-\sigma)) + \alpha^2\kappa\Omega\sin(\Omega\sigma), \end{aligned} \tag{32}$$

$$c(\Omega) = \beta\Omega^2\cos(\Omega\tau) - \alpha\kappa\Omega\sin(\Omega\tau) + \alpha^2\kappa\,. \tag{33}$$

For $\omega = 0$, the curve starts from $\beta_{-1} = -\kappa$, $\hat{\beta} = 0$, and it is singular at the roots of the $c(\Omega)$ function (see Fig. 4).

4.2 String stability

For the investigation of the string stability, let us again determine the transfer function $T(s) = N(s)/D(s)$, the numerator of which is

$$N(s) = (s\beta\hat{\beta} + \alpha\kappa\hat{\beta})\mathrm{e}^{-s\tau}\,, \tag{34}$$

while the denominator $D(s)$ takes the same form of the characteristic function (28).

The corresponding $\omega = 0$ string stability boundary is

$$\begin{aligned} \hat{\beta} &= \frac{-\beta_{-1}(\alpha+\beta-\kappa) + \alpha\kappa^2\sigma}{\alpha+2\beta-2\kappa} \\ &\pm \frac{\sqrt{(\beta_{-1}(\alpha+\beta-\kappa) - \alpha\kappa^2\sigma)^2 - \alpha(\alpha+2\beta-2\kappa)(\beta_{-1}+\kappa)^2}}{\alpha+2\beta-2\kappa}, \end{aligned} \tag{35}$$

which does not depend on the reaction time of the human driver.

Assuming $\alpha + \beta = \kappa$, the above expression simplifies to

$$\hat{\beta} = -\kappa^2\sigma \pm \sqrt{(\kappa^2\sigma)^2 + (\beta_{-1}+\kappa)^2}\,. \tag{36}$$

The $\omega > 0$ string stability boundary can be determined in closed algebraic form, but it leads again to a lengthy expression that is not presented here.

Figure 4 presents stability charts for various delay combinations in the plane of the control parameters β_{-1}, $\hat{\beta}$. The plant stable domain is bounded while its left boundary corresponding to low Ω frequencies is similar to the one generated without delays. The stable area shrinks significantly if the time delay of the AV increases, while the increase of the reaction time of the human driver has only a small effect, and it may even help in case of large $\hat{\beta}$ values (see panels (g) and (h)). The string stable region is primarily bounded by the $\omega = 0$ boundary from above, and an $\omega > 0$ boundary from the right, while around $\beta_{-1} = -\kappa$, $\hat{\beta} = 0$, there is a similar structure as it was showed for the delay-free case in Fig. 2.

5. DISCUSSION

An interesting question is how the automated vehicle behaves if a vehicle is driving behind it with constant velocity, in which case the steady state velocity of the automated vehicle is

$$v^\star = \frac{\hat{\beta}v_{\mathrm{ref}} + \beta_{-1}v_{-1}}{\hat{\beta} + \beta_{-1}}\,. \tag{37}$$

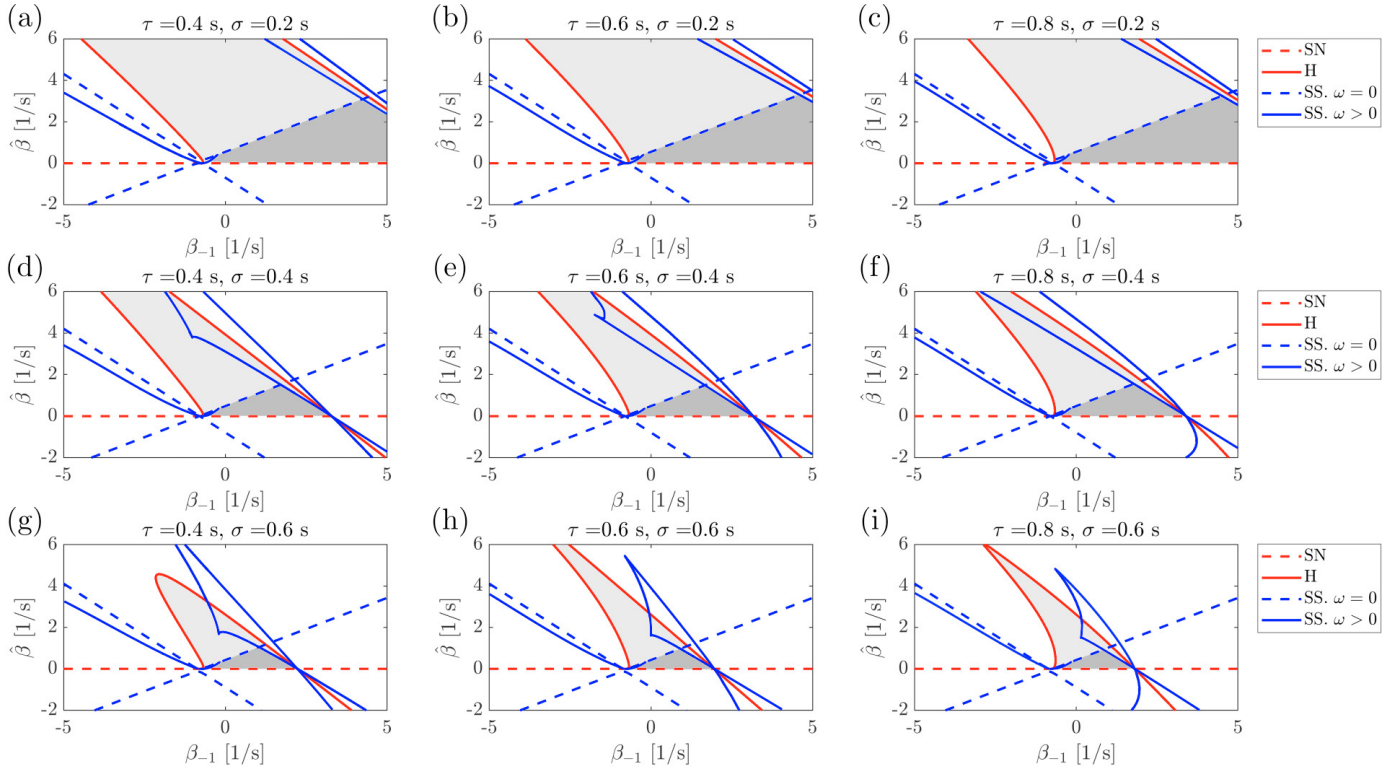

Fig. 4. Stability charts for various time delay combinations (for HV parameters $\alpha = 0.15$ 1/s, $\beta = 0.6$ 1/s, $\kappa = 0.8$ 1/s). The light and dark gray regions are both plant stable, while the dark gray area is string stable as well.

Introducing $\tilde{v} = v - v^\star$, the linearized equation of motion assumes the form of the Hayes equation (Stépán (1989)):

$$\dot{\tilde{v}}(t) = -(\hat{\beta} + \beta_{-1})\tilde{v}(t - \sigma)\,. \tag{38}$$

The corresponding saddle-node boundary is at

$$\hat{\beta} + \beta_{-1} = 0\,, \tag{39}$$

while the Hopf boundary curves take the form

$$\hat{\beta} = -\beta_{-1} + \frac{(2k+1)\pi}{2\sigma}(-1)^k\,, \quad k = 0, 1, 2\ldots. \tag{40}$$

Thus, the system is plant stable if

$$-\beta_{-1} < \hat{\beta} < -\beta_{-1} + \frac{\pi}{2\sigma}\,. \tag{41}$$

Figure 5 shows various stability charts for different delay combinations, where the upper limit of the plant stability region can be approximated well with the result of the Hayes equation. This is because the dynamic D-curve (30), intersects the $\hat{\beta}$ axis always when $\cos(\Omega\sigma) = 0$, and for the corresponding $\Omega = (2k+1)\pi/(2\sigma)$ value, one gets back the simple expression (40).

Based on Fig. 4, the right boundary of the string stable domain is close to the corresponding Hopf boundary and so it can also be approximated with the results of the Hayes equation (41). This provides a simple approximation for tuning the control parameters of the autonomous vehicle.

6. CONCLUSION

The paper investigated the guided control of a human-driven vehicle, ahead of which the automated vehicle is not only equipped with cruise control but it is sensing the

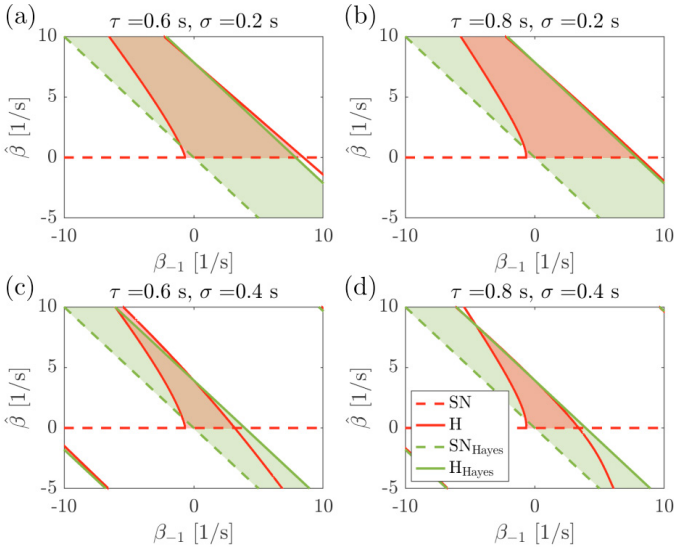

Fig. 5. Comparison of the stability chart of the original system (red) and stability chart when the HV travels with constant velocity (green).

distance and the relative velocity between the two cars and changes the applied actuation accordingly.

Neglecting the time delays, the stability charts showed that not only the whole positive quadrant of the β_{-1}, $\hat{\beta}$ plane is plant stable but the backward looking gain β_{-1} can be tuned even to negative values if the cruise control gain $\hat{\beta}$ is large enough. Furthermore, the string stable domains were determined as well, and stability charts are

presented for various values of the inverse κ of the time headway.

In Section 4, the relevant time delays were taken into account both for the HV and for the AV, which resulted bounded stable domains. Finally, the control of the AV was analyzed when the HV is traveling with constant speed behind it; the corresponding dynamics is described by the Hayes equation, which provides a quite good approximation of the upper stability boundary of the original system.

As a future work, we plan to analyze the nonlinear nature of the system and carry out experiments to verify the theoretical results.

ACKNOWLEDGEMENTS

The research reported in this paper has been supported by the Hungarian National Research, Development and Innovation Office (NKFI-KKP-133846 and NKFI-K-132477). GO acknowledges the support of the MTA distinguished fellowship of the Hungarian Academy of Sciences.

REFERENCES

Bando, M., Hasebe, K., Nakanishi, K., and Nakayama, A. (1998). Analysis of optimal velocity model with explicit delay. *Physical Review E*, 58(5), 5429.

Bekiaris-Liberis, N. and Delis, A.I. (2020). PDE-based feedback control of freeway traffic flow via time-gap manipulation of ACC-equipped vehicles. *IEEE Transactions on Control Systems Technology*, 29(1), 461–469.

Besselink, B. and Johansson, K.H. (2017). String stability and a delay-based spacing policy for vehicle platoons subject to disturbances. *IEEE Transactions on Automatic Control*, 62(9), 4376–4391.

Caveney, D. (2010). Cooperative vehicular safety applications. *IEEE Control Systems Magazine*, 30(4), 38–53.

Chan, E., Gilhead, P., Jelinek, P., Krejci, P., and Robinson, T. (2012). Cooperative control of SARTRE automated platoon vehicles. In *19th ITS World Congress*. Vienna.

Čičić, M. and Johansson, K.H. (2018). Traffic regulation via individually controlled automated vehicles: a cell transmission model approach. In *21st IEEE International Conference on Intelligent Transportation Systems*, 766–771.

Ge, J.I., Avedisov, S.S., He, C.R., Qin, W.B., Sadeghpour, M., and Orosz, G. (2018). Experimental validation of connected automated vehicle design among human-driven vehicles. *Transportation Research Part C*, 91, 335–352.

Laval, J.A. and Leclercq, L. (2013). The Hamilton–Jacobi partial differential equation and the three representations of traffic flow. *Transportation Research Part B*, 52, 17–30.

Lidström, K., Sjöberg, K., Holmberg, U., Andersson, J., Bergh, F., Bjäde, M., and Mak, S. (2012). A modular CACC system integration and design. *IEEE Transactions on Intelligent Transportation Systems*, 13(3), 1050–1061.

Loizou, S.G., Lui, D.G., Petrillo, A., and Santini, S. (2021). Connectivity preserving formation stabilization in an obstacle-cluttered environment in the presence of time-varying communication delays. *IEEE Transactions on Automatic Control*, 67(10), 5525–5532.

Milanés, V., Shladover, S.E., Spring, J., Nowakowski, C., Kawazoe, H., and Nakamura, M. (2013). Cooperative adaptive cruise control in real traffic situations. *IEEE Transactions on Intelligent Transportation Systems*, 15(1), 296–305.

Molnár, T.G., Upadhyay, D., Hopka, M., Nieuwstadt, M.V., and Orosz, G. (2021). Delayed Lagrangian continuum models for on-board traffic prediction. *Transportation Research Part C*, 123, 102991.

Molnár, T.G., Hopka, M., Upadhyay, D., Van Nieuwstadt, M., and Orosz, G. (2023). Virtual rings on highways: Traffic control by connected automated vehicles. In *AI-enabled Technologies for Autonomous and Connected Vehicles*, 441–479. Springer.

Molnár, T.G., Upadhyay, D., Hopka, M., Van Nieuwstadt, M., and Orosz, G. (2020). Open and closed loop traffic control by connected automated vehicles. In *59th IEEE Conference on Decision and Control*, 239–244.

Öncü, S., Ploeg, J., Van de Wouw, N., and Nijmeijer, H. (2014). Cooperative adaptive cruise control: Network-aware analysis of string stability. *IEEE Transactions on Intelligent Transportation Systems*, 15(4), 1527–1537.

Orosz, G. (2016). Connected cruise control: modelling, delay effects, and nonlinear behaviour. *Vehicle System Dynamics*, 54(8), 1147–1176.

Orosz, G. and Stépán, G. (2006). Subcritical Hopf bifurcations in a car-following model with reaction-time delay. *Proceedings of the Royal Society A*, 462(2073), 2643–2670.

Ploeg, J., Shukla, D.P., Van De Wouw, N., and Nijmeijer, H. (2013a). Controller synthesis for string stability of vehicle platoons. *IEEE Transactions on Intelligent Transportation Systems*, 15(2), 854–865.

Ploeg, J., Van De Wouw, N., and Nijmeijer, H. (2013b). Lp string stability of cascaded systems: Application to vehicle platooning. *IEEE Transactions on Control Systems Technology*, 22(2), 786–793.

Qin, W.B., Gomez, M.M., and Orosz, G. (2016). Stability and frequency response under stochastic communication delays with applications to connected cruise control design. *IEEE Transactions on Intelligent Transportation Systems*, 18(2), 388–403.

Stépán, G. (1989). *Retarded dynamical systems: stability and characteristic functions*. Longman.

Swaroop, D. and Hedrick, J.K. (1996). String stability of interconnected systems. *IEEE transactions on Automatic Control*, 41(3), 349–357.

Wang, J., Zheng, Y., Chen, C., Xu, Q., and Li, K. (2021). Leading cruise control in mixed traffic flow: System modeling, controllability, and string stability. *IEEE Transactions on Intelligent Transportation Systems*.

Wang, M., Hoogendoorn, S.P., Daamen, W., van Arem, B., Shyrokau, B., and Happee, R. (2018). Delay-compensating strategy to enhance string stability of adaptive cruise controlled vehicles. *Transportmetrica B*, 6(3), 211–229.

Yu, H., Koga, S., and Krstic, M. (2018). Stabilization of traffic flow with a leading autonomous vehicle. In *Dynamic Systems and Control Conference*, volume 51906, V002T22A006. ASME.